Pore-scale Spectral Induced Polarization (SIP) signatures associated with FeS biomineral transformations

Lee Slater[1], Dimitrios Ntarlagiannis[1#], Yves R. Personna[1] and Susan Hubbard[2]

1. Department of Earth & Environmental Sciences, Rutgers-Newark, New Jersey, USA
2. Lawrence Berkeley National Laboratory, Berkeley, California, USA

Now at School of Planning, Architecture and Civil Engineering, Queen's University Belfast, Belfast, UK

Abstract

We measured Spectral Induced Polarization (SIP) signatures in sand columns during (1) FeS biomineralization produced by sulfate reducing bacteria (D. vulgaris) under anaerobic conditions, and (2) subsequent biomineral dissolution upon return to an aerobic state. The low-frequency (0.1-10 Hz peak) relaxations produced during biomineralization can be modeled with a Cole-Cole formulation, from which the evolution of the polarization magnitude and relaxation length scale can be estimated. We find that the modeled time constant is consistent with the polarizable elements being biomineral encrusted pores. Evolution of the model parameters is consistent with FeS surface area increases and pore-size reduction during biomineral growth, and subsequent biomineral dissolution (FeS surface area decreases and pore expansion) upon return to the aerobic state. We conclude that SIP signatures are diagnostic of pore-scale geometrical changes associated with FeS biomineralization by sulfate reducing bacteria.

Introduction

Near surface geophysical measurements are potentially sensitive to microbial processes (see *Atekwana et al., 2006*, for review). Geophysics offers the possibility of observing microbial processes non-invasively, and at larger scales inaccessible with standard microbiological techniques. One microbial process detectable with electrical geophysical methods is iron sulfide (FeS) biomineralization induced by sulfate reducing bacteria (*Williams et al, 2005; Ntarlagiannis et al., 2005)*. The potential hence exists to monitor sulfide mineral formation processes in marine environments and wetlands, remediation of mine wastes using wetlands, and biostimulation strategies for the degradation of contaminants.

The spectral induced polarization (SIP) method measures the low-frequency (sub-kHz) electrical properties (related to both conduction loss and charge storage) of a porous medium (see *Lesmes and Friedman, 2005*, for review). The method was developed for locating buried metallic mineral deposits (e.g. massive FeS mineralization) based on a polarization phenomenon that occurs at the interface between metallic minerals and the pore-filling fluid (*Wong, 1979*). *Williams et al. (2005)* showed that the formation of FeS biominerals under anaerobic sulfate reducing conditions generates measurable (~15 mrad) SIP signals with central relaxation frequencies between 0.1-10 Hz. *Ntarlagiannis et al. (2005)* analyzed single frequency data from the same experiment and showed that the polarization magnitude is proportional to the rate of microbial activity. They suggested that changes in the relative strength of polarization and conduction results from a geometric rearrangement of evolved biominerals in pore spaces.

In this letter we extend this work by reporting results of a new column experiment whereby we first induce anaerobic FeS biomineralization but then subsequently induce biomineral dissolution by returning the system to an oxic state. We also model the SIP signature of both phases using a Cole-Cole

relaxation (*Cole and Cole, 1941*). We show that the SIP signal (and modeled dispersion parameters) generated during biomineralization is fully reversible and exhibits no significant hysteresis. Furthermore, we show that the time constant of the relaxation (and its temporal behavior during biomineral formation and dissolution) is consistent with the source of this polarization being biomineral encrusted pores of the sand matrix, and not the biomineral encrusted bacterial cells themselves.

Methods

The experiment design closely followed that described in *Williams et al. (2005)*. All materials were sterilized using common protocols. Quartzitic sand (grain size for which 50 % of sample is finer (d_{50}) = 0.3 mm; porosity = 37 ± 1 %), treated to remove trace organics and/or iron oxides, was packed into a horizontal column (diameter = 0.0317 m; length = 0.203 m) containing six Ag-AgCl electrodes housed in electrolyte-filled ports attached to the column edge. Two Ag-AgCl coils (diameter = 0.0317 m) were emplaced at column ends for current injection. The column was saturated and continually circulated with a growth medium (including lactate, sulfate, iron, minerals and vitamins) and purged with N_2 gas to remove residual air bubbles. A continuous flow rate of ~ 2 pore volumes/day (~0.4 m/day) was established with a peristaltic pump (maintained for the 55 days). Between Days 0-35 (anoxic phase) the column was placed in an anerobic chamber to facilitate microbial sulfate reduction. The anaerobic chamber was opened to the atmosphere on Day 36 until Day 55 to encourage FeS oxidation and dissolution. The growth medium was still continuously circulated (without sparing with N_2) but exposed to air via a 0.45 μm filter.

Cells of a pure culture of *Desulfovibrio vulgaris* (*D. vulgaris*) were grown and inoculated into the center of the experiment column via syringe on Day 5. Pore water samples for analysis of aqueous geochemistry were extracted by syringe at three locations along the column every 1-2 days following

66 inoculation. We measured Eh, pH, and electrolyte conductivity using bench-top probes. Lactate, acetate,
67 and sulfate were measured with an ion chromatograph. Hydrogen sulfide (H_2S) concentration was
68 estimated using a test kit (HACH HS-WR) immediately after sampling to minimize volatization of H_2S
69 to the atmosphere. The column solid phase was analyzed upon termination of the experiment at Day 55
70 using scanning electron microscopy (SEM).

71 SIP measurements were collected at 40 equally spaced (in log space) frequencies between 0.1-1000 Hz
72 using a dynamic signal analyzer (see *Slater and Lesmes, 2002* for details). Current was applied via the
73 coil electrodes, and impedance magnitude and phase shift (φ) recorded relative to a precision resistor.
74 This measurement was made at three locations along the column (between electrode pairs 1-2, 3-4 and
75 5-6) at 1-3 day intervals. The measurement error for the magnitude is less than 1% whereas the error in
76 φ is ~0.1 mrad below 100 Hz (*Slater and Lesmes, 2002*).

77 The SIP datasets were modeled with a phenomenological Cole-Cole dispersion expressed in terms of a
78 complex resistivity (ρ^*),

79 $$\rho^* = \rho_0\left[1 - m\left(\frac{1}{1+(i\omega\tau)^c}\right)\right], \qquad (1)$$

80 where ρ_0 is the dc resistivity, τ is the mean relaxation time associated with the frequency dispersion, c is
81 a shape exponent (0.2-0.8 for unconsolidated soils) and m is the chargeability associated with the
82 interfacial charge storage (*Pelton et al., 1978*). Model parameters were estimated using an algorithm
83 employing a least-squares approach with Marquardt regularization (*Kemna, 2000*). This algorithm
84 automatically nests a second higher-frequency relaxation (usually to model coupling effects in field
85 data). As the SIP frequency range is usually not wide enough to capture the shape of the second
86 relaxation we only report the parameters for the primary relaxation here. We recognize that Cole-Cole

87 parameter estimation is uncertain and may find local minima in the objective function. However,
88 analysis of parameter uncertainty suggested that τ is the most well resolved parameter (estimated
89 variances being less than 8 % of the parameter estimate).

90 **Results**

91 Figure 1 summarizes the aqueous geochemistry of the system (average values for the samples extracted
92 from the three sampling ports along the column) over the 55 days of the experiment. We define three
93 system states: (1) the anaerobic transition (t = 14-25 days); (2) the anaerobic phase (t = 26-35 days); (3)
94 the aerobic transition (t = 36-45 days). The anaerobic transition represents the onset of biomineralization
95 (following a ~2-3 day lag phase) as evidenced by decreasing sulfate (electron acceptor), decreasing
96 lactate (carbon source), increasing acetate (reaction byproduct) and increasing H_2S (reaction byproduct)
97 due to sulfate reduction. The aqueous H_2S produced from microbial induced sulfate reduction,
98 commonly reacts with any metals in solution forming metal sulfides (solid state). In our column the
99 dominant metal in solution is Fe^{2+} (125 μm inflow concentration) and the precipitating sulfide is FeS,

100 $$Fe^{2+} + H_2S_{(aq)} \rightarrow FeS_{(s)} + 2H^+ \qquad (2)$$

101 The anaerobic phase is characterized by relatively stable, low levels of lactate and sulfate but high levels
102 of acetate and H_2S. This phase represents maximum rates of microbial activity and coincided with
103 maximum visible precipitate formation, interpreted to be $FeS_{(s)}$. The black precipitate was visible
104 throughout the column by Day 10 and confirmed (via SEM supported with Energy Dispersive X-ray) as
105 FeS biomineralization.

106 The aerobic transition represents the return of the system to oxic conditions. Oxidation of FeS
107 over a ~10 day period (Day 36-45) is supported by previous laboratory studies confirming rapid rates of
108 pyrrhotite ($Fe_{(1-x)}S$, $0.0<x<0.125$) oxidation at atmospheric concentrations of O_2 and at 22° C, being

~100 times those measured for pyrite (FeS_2) (*Nicholson and Scharer,1994*). The return of H_2S to levels comparable to the start of the experiment is consistent with decreased sulfate reduction rates by *D. vulgaris* (and possibly chemical oxidation of sulfide). However, sulfate does not rebound completely, suggesting the continuation of sulfate-consuming anaerobic conditions in parts of the column. This is consistent with the known tolerance of *D. vulgaris* in microaerophillic (even in aerobic) conditions, it being likely that cells survived the aerobic transition, albeit with reduced activity. The aerobic transition was directly visible from the disappearance (dissolution) of the black FeS precipitate during this period. Continually low levels of lactate and the removal of acetate during the aerobic transition may reflect consumption by aerobic microbes unintentionally introduced to the column upon exposure to air.

In this letter we present only the results for electrode pair 5-6, which exhibited the most pronounced geoelectrical changes. A full analysis of the spatial variability in the geoelectrical data, and its correlation with spatially variable biomineral formation, will be presented in a forthcoming paper. Consistent with the results of *Williams et al. (2005)*, FeS biomineralization results in the development of a dispersive relaxation. Figure 2 is a plot of resistivity magnitude ($|\rho|$) and phase (φ) as a function of frequency at $t = 21$ days (anaerobic transition) illustrating this dispersion and showing the fit of Equation 1. The data are truncated at 100 Hz as above this frequency φ is less than the instrument accuracy (0.1 mrad). The open squares/circles are the measurements, and the lines depict the dispersion model fit. The model fits the data well (RMS error between model and data = 9 %) except below 0.1 Hz (most obvious in the $|\rho|$ term due to the fine plotting scale), which may suggest the presence of a very low frequency relaxation just captured in this dataset. The modeled time constant for the primary relaxation is 0.22 s (see caption in Figure 2 for other model parameters).

The temporal character of the SIP signature of this biomineralization process is demonstrated for the anaerobic transition and aerobic transition stages in Figure 3a and 3b respectively. Data points where the

$\varphi < 0.1$ mrad (instrument accuracy) are again omitted. Figure 3c shows the temporal evolution of the estimated dispersion model parameters $m_n = m/\rho_0$ (being the polarization strength e.g. *Lesmes and Frye, 2001*) and τ obtained for these datasets. Note that a satisfactory model could not be fit to the Day 14 dataset due to the very small polarization peak (~1.5 mrad). The anaerobic transition is characterized by an increase in the dispersion strength (i.e. increase in phase peak in data and m_n from model) and shift in phase peak to higher frequencies (decrease in τ from model). The aerobic transition shows essentially the reverse behavior as evidenced in the data (Figure 3b) and the modeled parameters (Figure 3c).

Post experimental destructive analysis followed by SEM imaging indicated the presence of biominerals (Figure 4a) and biofilms on quartz grains (Figure 4b). Energy dispersive microscopy (EDS) analysis showed that both biominerals and biofilms are composed of FeS. The FeS encrusted cells (Figure 4a) show the characteristic curved rod shape of *D. vulgaris* with an average size of 0.44 ±0.06 μm and 1.93 ± 0.15 μm (based on three SEM images) in the short and long axis, respectively.

Discussion

The SIP response of FeS biomineralization can be modeled with a Cole-Cole model with τ in the range of 0.2-0.4 s (Figure 3c). We find that the SIP response that develops during the transition to sulfate reducing conditions and biomineral formation (anaerobic transition) is reversible, exhibiting no significant evidence of hysteresis, upon biomineral dissolution during the return to oxic conditions (aerobic transition). This suggests that the SIP method could be used to monitor and track not only variable rates, but also variable directions, of microbial-mineral transformations in environments where redox conditions fluctuate.

Although purely a phenomenological approach, the Cole-Cole modeling affords insights into the polarization mechanism associated with this process. It is recognized that τ is inversely related to some

154 measure of the length scale over which ions in the electrical double layer at the mineral-fluid interface
155 are displaced. *Schwarz (1962)* provides a model for the polarization of a particle in a uniform electrical
156 field, based on tangential ionic fluxes, whereby the time constant of the relaxation is related to the
157 particle radius (r),

158 $$\tau = \frac{r^2}{2D}, \qquad (3)$$

159 where D is the surface ionic diffusion coefficient (in m^2s^{-1}). Values of D are uncertain but are often
160 considered to be an order of magnitude smaller than the diffusion coefficient for the bulk solution ($\sim 10^{-9}$
161 m^2s^{-1}).

162 *Tarasov and Titov (2007)* performed SIP measurements on sands with a well defined, narrow grain size
163 distribution and estimated D as $\sim 3x10^{-9}$ m^2s^{-1}. Table 1 shows the equivalent polarizable particle
164 diameter for the two end members of the modeled τ range shown in Figure 3c based on this value of D.
165 The estimated diameters (0.07-0.10 mm) are almost two orders of magnitude larger than the long axis
166 (approaching three orders of magnitude larger than the short axis) of the FeS encrusted, *D. vulgaris*
167 biominerals (Fig 4a). Despite the simplicity of the model (the tubular biominerals in Fig 4a are not
168 spherical particles, uncertainty in the magnitude of D), this discrepancy suggests that the dispersion
169 between 0.1-100 Hz is not the relaxation associated with polarized biomineral encrusted bacteria
170 themselves. We recognize the uncertainty inherent in the parameter estimates, but stress that we could
171 reach similar conclusions using the raw data alone (i.e. the magnitude of the phase peak [in place of m_n]
172 and $1/f_c$ [f_c being the critical relaxation frequency] in place of τ).

173 The particle size estimated from Equation 3 is close to (about 3 times smaller than) the d_{50} of the
174 quartzitic sand particles used in this study (Table 1). We therefore suggest that the SIP relaxation
175 observed here (and by *Williams et al., 2005*) likely results from the formation of FeS biofilms

176 (coagulation of individual biominerals) on the mineral surface of pores in the sand matrix. An example
177 of this FeS biofilm forming on a quartzitic sand grain is shown in Figure 4b. We thus interpret the basic
178 polarizable element to be the biomineral encrusted pores, having similar dimensions to the grains.

179 This polarizable pore model can conceptually explain the change in τ and m_n (or from the data, $1/f_c$ and
180 magnitude of phase peak) observed during the anaerobic, and subsequent aerobic, transitions. The
181 variation in m_n is consistent with this model as m_n is a measure of the amount of polarizable surface area
182 (*Lesmes and Friedman, 2005*). The increase in m_n during the anaerobic transition is consistent with an
183 increase in FeS-fluid interfacial area resulting from biomineralization growth within the pore space. The
184 reverse behavior during the subsequent aerobic transition is then expected given the subsequent
185 biomineral dissolution and loss of FeS-pore fluid interfacial area. The decrease in τ (and hence r) during
186 the anaerobic transition is consistent with a shift to a smaller average polarizable pore size as the FeS
187 lining the pores thickens. The reverse behavior is then observed in the aerobic transition as FeS
188 dissolution starts at the biomineral-fluid interface and progressively enlarges the pores back to their
189 original sizes. We note that such direct relation between τ and m_n could conceivably break down if FeS
190 mineralization continued such that pores became so extensively filled with FeS that FeS-fluid interfacial
191 area started to decline. Visual observations of the column (and flow rates) suggest that such extensive
192 biomineralization was avoided.

193 We conclude that SIP signatures are likely diagnostic of pore-scale geometrical changes associated with
194 FeS biomineralization in pores by sulfate reducing bacteria. These signatures appear reversible (within
195 the accuracy of the measurement) following subsequent biomineral dissolution. The estimates of
196 polarizable element (i.e. biomineral-modified pore) size are uncertain, although the opportunity to
197 reduce this uncertainty may exist using Bayesian estimation procedures (*Chen et al., 2007*). Our work

highlights the opportunity that exists to improve understanding of biogeochemical processes using geophysical measurements that could be deployed from boreholes or the ground surface.

Acknowledgements

This study was funded by the Department of Energy, Environmental Remediation Sciences Program (ERSP) grant 1027674 to S. Hubbard. This material is also based upon work supported by the National Science Foundation under Grant No. 0433739. Andreas Kemna provided the Cole-Cole relaxation modeling algorithm used here.

206

207 **References**

208 Atekwana, E., D.D. Werkema, Jr. and E. Atekwana (2006), Biogeophysics: The effects of microbial
209 processes on geophysical properties of the shallow subsurface, In, Vereeken, H., Binley, A., Cassiani, G,
210 Revil, A. and Titov, K., Eds., "Applied Hydrogeophysics", NATO Science Series IV: Earth and
211 Environmental Sciences, Springer, 161-193.

212 Chen, J., S. Hubbard, K. Williams, A. Kemna, L. Slater and S. Pride (2006), A Stochastic Framework
213 for Geochemical Parameter Estimation using Geophysical Methods: Development and Application, Eos
214 Trans. AGU, 87(52), Fall Meet. Suppl., Abstract H44B-04.

215 Cole, K.S. and R.H. ole (1941), Dispersion and absorption in dielectrics, vol. I. Alternating current field.
216 *Journal of Chemical Physics*, *9*: 341-351.

217 Kemna, A. (2000), Tomographic inversion of complex resistivity - theory and application, Der Andere
218 Verlag, Osnabrück, Germany, 176 pp

219 Lesmes, D.P. and K.M. Frye (2001), The influence of pore fluid chemistry on the complex conductivity
220 and induced-polarization responses of Berea sandstone, *Journal of Geophysical Research, 106*(B3),
221 4079-4090.

222 Lesmes, D. P. and S.P. Friedman (2005), Relationships between the electrical and hydrogeological
223 properties of rocks and soils. in Hydrogeophysics, edited by Rubin, Y and Hubbard S. S., Chap. 4,, pp.
224 87-128, Springer, Dordrecht, The Netherlands.

225 Nicholson, R.V. and J.M. Scharer, J.M. (1994), Laboratory studies of pyrrhotite oxidation kinetics, In:
226 Alpers, C.N. and D.W. Blowes, Eds, Environmental Geochemistry of Sulfide Oxidation. ACS
227 Symposium Series, vol. 550, pp. 14-30. Washington, DC.

228 Ntarlagiannis, D., K.H. Williams, L. Slater and S. Hubbard (2005), The low frequency electrical
229 response to microbially induced sulfide precipitation, *Journal of Geophysical Research, 110*, G02009.

230 Pelton, W.H., S.H. Ward, P.G. Hallof, W.R. Sill and P.H. Nelson (1978), Mineral discrimination and
231 removal of inductive coupling with multifrequency IP, *Geophysics, 43*, 588-609.

232 Schwarz, G. (1962), A theory of the low-frequency dielectric dispersion of colloidal particles in
233 electrolyte solution, *Journal of Physical Chemistry, 66*(12): 2636-2642.

234 Slater, L. and D.P. Lesmes (2002), Electrical-hydraulic relationships observed for unconsolidated
235 sediments, *Water Resources Research, 38*(10), 1213.

236 Tarasov, A. and T. Titov (2007), Relaxation time distribution from time domain induced polarization
237 measurements, *Geophysical Journal International, 170*, 31-43.

238 Williams, K.H., D. Ntarlagiannis, L. Slater, A. Dohnalkova, S.S. Hubbard and J.F. Banfield (2005),
239 Geophysical imaging of stimulated microbial biomineralization, *Environmental Science & Technology*,
240 *39*(19), 7592-7600.

241 Wong, J. (1979), An electrochemical model of the induced-polarization phenomenon in disseminated
242 sulfide ores. *Geophysics*, *44*: 1245-1265.

243

244

245 **Table captions**

246 Table 1: Comparison of SIP estimated radii (r) of polarizable spheres with sand grain size from sieve
247 analysis and biomineral size from SEM imaging.

248 **Figure captions**

249 Figure 1: Aqueous geochemistry of column effluent. Anaerobic and aerobic transitions when SIP data
250 were collected are shaded.

251 Figure 2: Spectral Induced Polarization signature of FeS biomineralization at 21 days showing both
252 phase (φ) and magnitude (|ρ|) response. The fit of the data to a Cole-Cole model is also shown. The
253 Cole-Cole parameters for this model are $\rho_0 = 39.1$ Ohm m; $m = 0.025$; $\tau = 0.22$ s; $c = 0.76$. Open
254 symbols = measured data; Solid lines = model fit; The x-axis is truncated at 100 Hz as the response
255 between 100-1000 Hz is below the 0.1 mrad instrument accuracy. The rms misfit between the model and
256 measured data is 9 %.

257 Figure 3: Measured phase ($-\varphi$) data as a function of time (a) Anaerobic transition between 14-25 days
258 (b) Aerobic transition between 36-45 days. The data are truncated at a value of -0.1 mrad (the accuracy
259 of the instrument). (c) Variation of modeled Cole-Cole parameters as a function of time (black circles =
260 τ; open circles = m_n)

261 Figure 4: Examples of scanning electron microscope (SEM) images captured upon destructive analysis
262 of the column at the end of the experiment (t = 55 days) (a) FeS encrusted *D. vulgaris* biomineral The
263 approximate dimensions of these elongate, tube-like biominerals (average dimensions based on three

264 cells captured in three separate images) are 1.93+-0.15 μm by 0.44 +- 0.06 μm. (b) Quartz sand particle
265 encrusted with FeS biomineralization.
266

Table 1: Comparison of SIP estimated radii (r) of polarizable spheres with sand grain size from sieve analysis and biomineral size from SEM imaging.

D^* (m^2s^{-1})	τ (s)	$2r^{\#}$ (mm)	Sand $d_{50}{}^{\$}$ (mm)	Biomineral† *long axis (mm)*	*short axis (mm)*
3.00E-09	0.4	0.10	0.30	0.0019	0.0004
3.00E-09	0.2	0.07			
				± 0.0001‡	*± 0.0001*‡

** after Tarasov & Titov (2007); # calculated from Equation 3; $ from sieve analysis, † from SEM images; ‡ calculated from standard deviation of measurements on three biominerals*

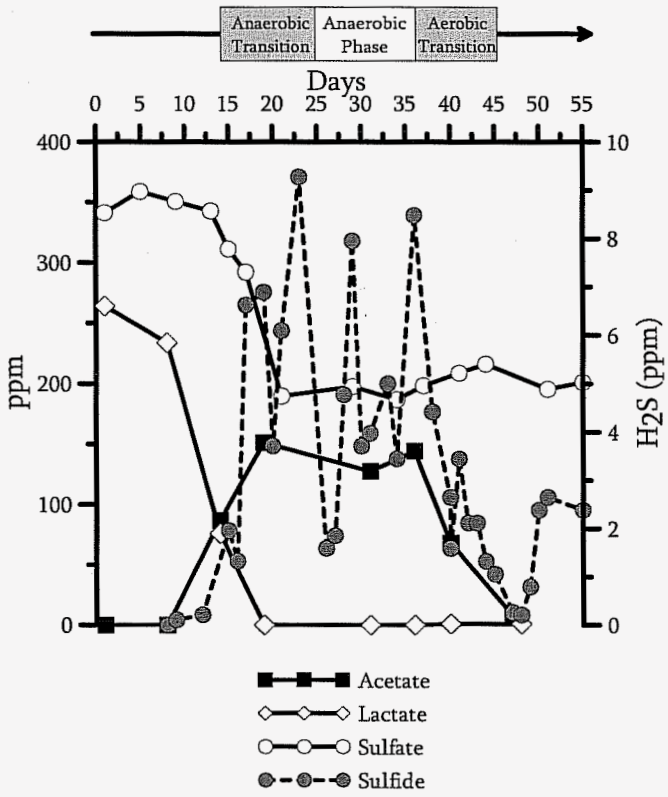

Figure 1: Aqueous geochemistry of column effluent. Anaerobic and aerobic transitions when SIP data were collected are shaded. Lactate, acetate and sulfate are plotted on the left y-axis where sulfide is plotted on the right y-axis.

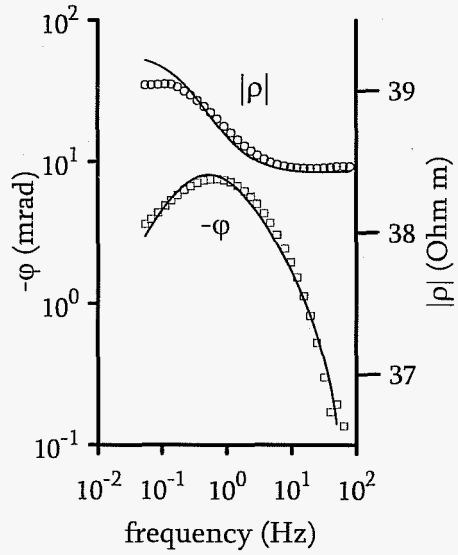

Figure 2: Spectral Induced Polarization signature of FeS biomineralization at 21 days showing both phase (φ) and magnitude ($|\rho|$) response. The fit of the data to a Cole-Cole model is also shown. The Cole-Cole parameters for this model are $\rho_0 = 39.1$ Ohm m; $m = 0.025$; $\tau = 0.22$ s; $c = 0.76$. Open symbols = measured data; Solid lines = model fit; The x-axis is truncated at 100 Hz as the response between 100-1000 Hz is below the 0.1 mrad instrument accuracy. The rms misfit between the model and measured data is 9 %.

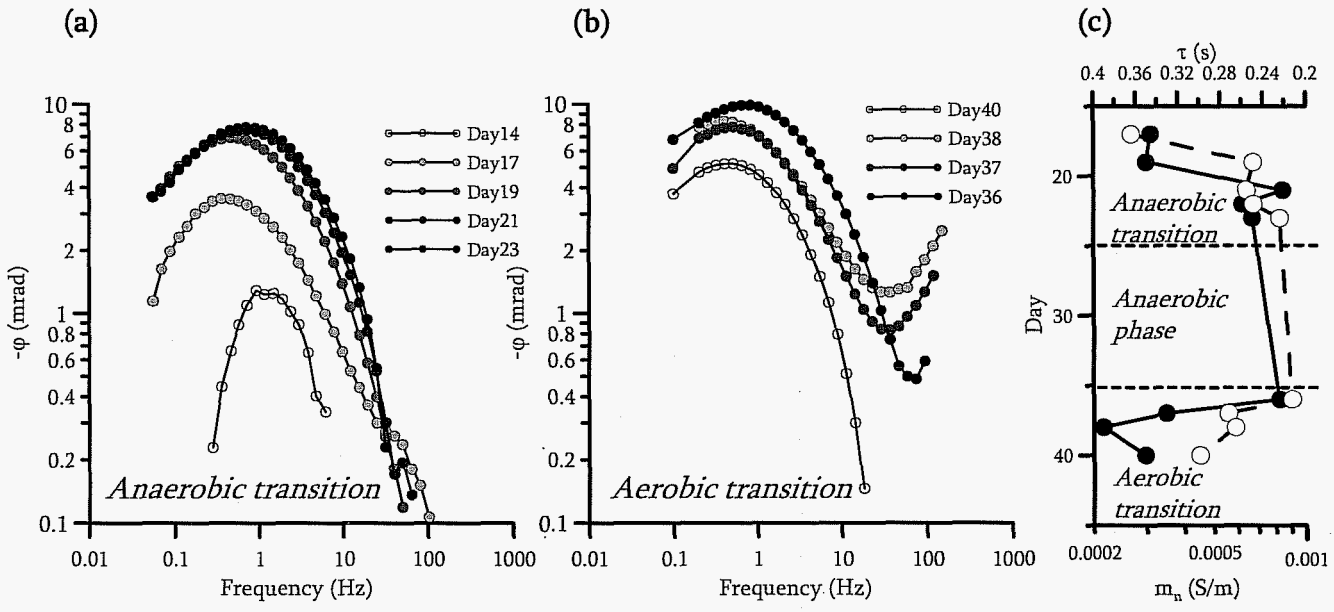

Figure 3: Measured phase (-ϕ) data as a function of time (a) Anaerobic transition between 14-25 days (b) Aerobic transition between 36-45 days. The data are truncated at a value of -0.1 mrad (the accuracy of the instrument). (c) Variation of modeled Cole-Cole parameters as a function of time (black circles = τ; open circles = m_n)

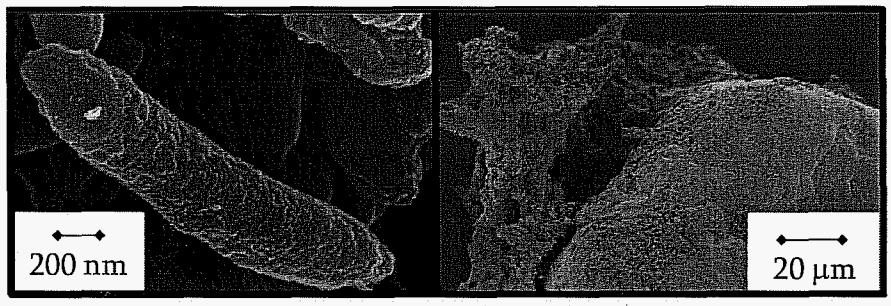

Figure 4: Examples of scanning electron microscope (SEM) images captured upon destructive analysis of the column at the end of the experiment (t = 55 days) (a) FeS encrusted *D. vulgaris* biomineral The approximate dimensions of these elongate, tube-like biominerals (average dimensions based on three cells captured in three separate images) are 1.93+-0.15 μm by 0.44 +- 0.06 μm. (b) Quartz sand particle encrusted with FeS biomineralization.